

Bifurcations in Rayleigh-Benard Convection

A Major Qualifying Project Report:

Submitted to the Faculty

Of the

Worcester Polytechnic Institute

in partial fulfillment of the requirements for the

Degree of Bachelor of Science

by

David LeRay

Date: May 20, 2004

Approved:

Professor Homer Walker, Major Advisor

Professor William Farr, Co-Advisor

Professor Joseph Fehribach, Co-Advisor

Contents

1	Introduction	1
2	Background	2
2.1	Rayleigh-Benard Convection	2
2.2	Symmetries of the equations and linear stability analysis	4
2.2.1	Symmetries of the equations	4
2.2.2	Linear stability analysis	5
2.3	Numerical algorithms and methods	5
2.3.1	Newton's method	5
2.3.2	Inexact Newton's method	6
2.3.3	Globalization techniques	6
2.3.4	Solving the linear Newton equation	7
2.3.5	Preconditioning	7
3	Methodology	9
3.1	Discretization overview	9
3.1.1	Discretization of the temperature	9
3.1.2	Discretization of ψ , the stream function	9
3.1.3	Discretization of ω , vorticity	10
3.2	Preconditioning	10
4	Results	12
4.1	Summary of linear stability results	12
4.2	Solution	14
4.2.1	The presence of two convection solutions	15
4.3	Symmetries in the solution	15
4.4	Bifurcation results	17
4.4.1	Temperature amplitude as a function of Ra	17
4.4.2	Variation in aspect ratio, with a constant Ra	17
4.5	Animation program	18
5	Conclusions and Future Work	20
5.1	Conclusions	20
5.2	Future Work	20

List of Figures

2.1	Rayleigh-Benard convection	2
3.1	The effect of preconditioning on INB	11
3.2	The effect of preconditioning on GMRES	11
4.1	Curves of neutral stability under variables R and γ	12
4.2	Sketches of solutions at various Ra and aspect ratio [6]	13
4.3	Solution obtained at various Ra and γ	14
4.4	The two convection solutions	15
4.5	ψ of mode 1 as found with the computer simulation	15
4.6	T of mode 1 as found with the computer simulation	16
4.7	ψ of mode 2 as found with the computer simulation	16
4.8	T of mode 2 as found with the computer simulation	16
4.9	Amplitude of temperature pertubation as a function of Rayleigh number	17
4.10	Qualitative graph of neutral stability curves under variables R and γ	18
4.11	A “journey” across various γ for $Ra = 3500$	18
4.12	Screenshot of the animation program	19

List of Tables

2.1	The symmetries of a rectangle	4
2.2	The symmetries of the Rayleigh-Benard system	4
4.1	Rayleigh number conversion table	14

Chapter 1

Introduction

Thermal convection is the flow of fluid induced by a temperature difference, or gradient. Thermal convection has been studied for the past two hundred years, but analytical solutions are lacking for many important situations [1].

Rayleigh-Benard convection is a particular type of thermal convection problem. Consider a rectangular domain that is insulated on the sides and heated on the bottom, creating a vertical temperature gradient. By the laws of thermal expansion, the fluid on the bottom is less dense than that on the top, creating a potentially unstable situation. Gravity imposes a downward force on the fluid, while the heat transfer imposes an upward force. A variation on this problem was originally considered by Lord Rayleigh in the early 1900's, with an attempted explanation of the problem published in a 1916 article.

This project dealt with solving the problem numerically, as well as some analysis of the bifurcation properties of the system. The project began with the formulation of a mathematical model. In order to model this situation, the Navier-Stokes equations were used, with the Boussinesq approximation. This approximation states that the density of the fluid can be considered constant in every term of the equations except those terms associated with the external force of gravity.

The equations that arise from the model were then solved numerically. The partial differential equations were discretized using finite differences on a regularly spaced rectangular grid. The nonlinear algebraic equations were solved using a globalized inexact Newton method, with an advanced linear solver used to determine the Newton step. The number of equations in these numerical trials was in the ten-thousands.

Once the computer code was working to our satisfaction, the tracking of solutions began. Variations in two system parameters were taken into account, the "Rayleigh number" and the aspect ratio of domain length to height. These results are discussed in a later section of the report.

Chapter 2

Background

2.1 Rayleigh-Benard Convection

Consider the following physical situation. There is a rectangular domain filled with fluid, with two parallel plates set horizontally above and below. The lower plate is kept constant at some temperature T_{hot} , while the upper plate remains at a colder temperature, T_{cold} ; the sides are insulated. Under high temperature gradients, the situation gives rise to a flow known as Rayleigh-Benard convection. Figure 2.1 demonstrates the physical situation. In the non-dimensional case, the value of y is one, while the value of x is allowed to vary with length L . The aspect ratio γ is defined as the ratio of L/H , which in the non-dimensional case is L .

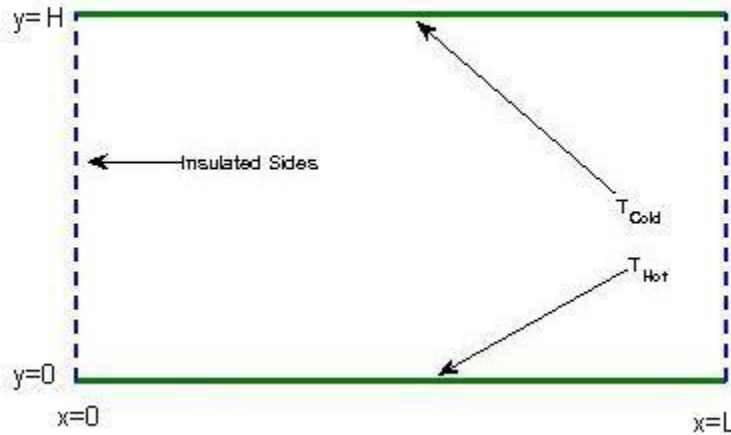


Figure 2.1: Rayleigh-Benard convection

The equations used to model the temperature profile and the fluid's motion are the continuity equation, the Navier-Stokes equation, and the thermal energy equation, which are (2.1), (2.2), and (2.3), with ρ as density, \vec{v} as velocity, P as pressure, \vec{g} as the gravity vector with magnitude g , T as temperature, C_p as the heat capacity, and k as the thermal conductivity.

$$\frac{\partial \rho}{\partial t} + \rho \nabla \cdot \vec{v} = 0 \quad (2.1)$$

$$\rho \frac{\partial \vec{v}}{\partial t} + \rho \vec{v} \cdot \nabla \vec{v} = -\nabla P + \rho \vec{g} + \nabla \cdot T \quad (2.2)$$

$$\rho C_p \frac{\partial T}{\partial t} + \rho C_p \vec{v} \cdot \nabla T = k \Delta T \quad (2.3)$$

If Rayleigh-Benard convection is not present in the solution (due to system parameters), the solution of the equations is a linear temperature profile with $\vec{v} = 0$, which is the conduction solution.

In the context of the physical problem, several assumptions can be made, known as the Boussinesq approximations:

1. The fluid is incompressible: $\nabla \cdot \vec{v} = 0$.
2. Thermal conductivity, viscosity, and C_p are all constants.
3. Variation of ρ is only significant in the buoyancy term $\rho \vec{g}$ (where it can't be assumed constant). Otherwise $\rho = \rho_o$, the fluid density at T_{hot} .
4. The equation for ρ is linear with respect to temperature; this can be expressed as in (2.4).

$$\rho = \rho_o(1 - \alpha(T - T_{hot})) \quad (2.4)$$

5. Viscous dissipation is negligible: $\nabla \cdot T = \mu \Delta \vec{v}$

Defining κ , the thermal diffusivity, as (2.5), and ν , the kinematic viscosity as (2.6), we arrive at (2.7), (2.8), and (2.9) .

$$\kappa = \frac{k}{\rho_o C_p} \quad (2.5)$$

$$\nu = \frac{\mu}{\rho_o} \quad (2.6)$$

$$\nabla \cdot \vec{v} = 0 \quad (2.7)$$

$$\frac{\partial \vec{v}}{\partial t} + \vec{v} \cdot \nabla \vec{v} = \frac{-1}{\rho_o} \nabla P + (1 - \alpha(T - T_{hot})) \vec{g} + \nu \Delta \vec{v} \quad (2.8)$$

$$\frac{\partial T}{\partial t} + \vec{v} \cdot \nabla T = \kappa \Delta T \quad (2.9)$$

Now, by subtracting out the conduction solution from the equations, and making the equations dimensionless (using the variables Ra and P_r as defined in (2.10) and (2.11)), we arrive at the final form of the equations, as found in (2.12), (2.13), and (2.14). The temperature in these equations represents the deviation from the conduction solution; \vec{e}_2 is a unit vector parallel to the temperature gradient. In the computations, only the steady-state solution is being sought, so the time derivatives were also set to zero.

$$P_r = \frac{\nu}{\kappa} \quad (2.10)$$

$$Ra = \frac{\alpha g (T_{hot} - T_{cold}) H^3}{\nu \kappa} \quad (2.11)$$

$$\nabla \cdot \vec{v} = 0 \quad (2.12)$$

$$\frac{1}{P_r} (\vec{v} \cdot \nabla \vec{v}) = -\nabla P + Ra T \vec{e}_2 + \Delta \vec{v} \quad (2.13)$$

$$\vec{v} \cdot \nabla T - \vec{v} \cdot \vec{e}_2 = \Delta T \quad (2.14)$$

Description	Group Element	Action
x reflection	κ_1	$(x, y) \rightarrow (L - x, y)$
y reflection	κ_2	$(x, y) \rightarrow (L - x, 1 - y)$
Rotation by 180	$\kappa_1\kappa_2$	$(x, y) \rightarrow (L - x, 1 - y)$

Table 2.1: The symmetries of a rectangle

Group Element	Action		
1	$\psi(x, y, t)$	$\omega(x, y, t)$	$T(x, y, t)$
κ_1	$-\psi(L - x, y, t)$	$-\omega(L - x, y, t)$	$T(x, y, t)$
κ_2	$-\psi(x, 1 - y, t)$	$-\omega(x, 1 - y, t)$	$T(x, 1 - y, t)$
$\kappa_1\kappa_2$	$\psi(L - x, 1 - y, t)$	$\omega(L - x, 1 - y, t)$	$-T(L - x, 1 - y, t)$

Table 2.2: The symmetries of the Rayleigh-Benard system

Now, by taking the curl of (2.13), and introducing both ψ , the stream function, satisfying (2.15) and (2.16), and ω , the vorticity, we arrive at the final form of the equations used in the model, (2.17), (2.18), and (2.19). This version of the Navier-Stokes equations is known as the stream-function vorticity form. In these equations, the unknowns are ψ, ω , and T .

$$\frac{\partial \psi}{\partial y} = u \quad (2.15)$$

$$\frac{\partial \psi}{\partial x} = -v \quad (2.16)$$

$$\frac{1}{Pr} \left(\frac{\partial \psi}{\partial y} \frac{\partial}{\partial x} - \frac{\partial \psi}{\partial x} \frac{\partial}{\partial y} \right) \omega = \text{Ra} \frac{\partial T}{\partial x} + \Delta \omega \quad (2.17)$$

$$\frac{\partial \psi}{\partial y} \frac{\partial T}{\partial x} - \frac{\partial \psi}{\partial x} \frac{\partial T}{\partial y} = -\frac{\partial \psi}{\partial x} + \Delta T \quad (2.18)$$

$$\Delta \psi = -\omega \quad (2.19)$$

The boundary conditions can be expressed mathematically in these equations as in the following list:

- $y = 0 : T = 0, u = 0, \psi = 0, \omega = -\frac{\partial u}{\partial y}, 0 < x < L$
- $y = 1 : T = 0, u = 0, \psi = 0, \omega = -\frac{\partial u}{\partial y}, 0 < x < L$
- $x = 0 : \frac{dT}{dx} = 0, v = 0, \psi = 0, \omega = \frac{\partial v}{\partial x}, 0 < y < 1$
- $x = L : \frac{dT}{dx} = 0, v = 0, \psi = 0, \omega = \frac{\partial v}{\partial x}, 0 < y < 1$

2.2 Symmetries of the equations and linear stability analysis

2.2.1 Symmetries of the equations

It is important to know and understand the symmetries in the system equations because steady bifurcating branches will be fixed by one of the elements of D_2 , the group of symmetries of a rectangle, provided it can be proved that the eigenvalues are real. I will not explain the proof of this here, but for reference I would suggest [1]. The elements of D_2 are found in Table 2.1. Remember, in the dimensionless form, the height is always set to 1 while the length of the domain can vary as $x = L$.

The symmetries that are present in the Rayleigh-Benard equations are found in Table 2.2.

2.2.2 Linear stability analysis

To determine parameter regions of Ra and aspect ratio γ where a non-zero stable solution can be found, it was necessary to calculate the “Neutral Stability Curve”. The basic idea is linearize the non-linear equations, create trial solutions based on the symmetries known to be present in the system as well as the boundary conditions (these would be similar to the actual steady non-zero solution), plug the trial solutions into the equations, and “backsolve” for the Rayleigh number and aspect ratio that were used to obtain the solution.

The linearized equations are found in (2.20) and (2.21) (the third equation has been used to eliminate ω).

$$0 = Ra \frac{\partial T}{\partial x} - \Delta^2 \psi \quad (2.20)$$

$$0 = -\frac{\partial \psi}{\partial x} + \Delta T \quad (2.21)$$

One could then use trial functions for T and ψ to calculate initial guesses for Newton’s method that would satisfy the boundary conditions and the symmetries present in the solution, and that would be close to the actual solution. However, in our case, it turns out an initial guess of a constant solution across the domain would also converge to the convection solutions, so this type of analysis is not necessary.

2.3 Numerical algorithms and methods

2.3.1 Newton’s method

Newton’s method is a numerical algorithm used to solve non-linear problems. The basic outline is as follows:

1. Given x
2. Solve $F'(x)s = -F(x)$ for s , which is the Newton equation
3. Update $x \leftarrow x + s$ and repeat

By theory in numerical analysis, quadratic convergence can be expected for this method, provided the initial guesses are close enough to the solution and F satisfies some mild assumptions [3]. This idea is presented mathematically as (2.22).

$$\|x_{k+1} - x_*\| \leq \beta \|x_k - x_*\|^2 \quad (2.22)$$

At first glance, this seems like a basic algorithm; however, there are many refinements that can be done to streamline the algorithm and make it more effective on certain problems. The three main questions to address in Newton’s method are:

1. The linear Newton equation could possibly be solved approximately using an iterative solver. This implies that the solution will not be an exact algebraic solution. How should the algorithm be modified to account for this?
2. What happens if the initial guess isn’t near the solution? Is there any way to modify the algorithm to ensure significant progress towards a solution?
3. Given that an iterative solver is a possibility, what would be the best solver to use?

2.3.2 Inexact Newton's method

The first question can be addressed by loosening the definition of “solve” in Newton algorithm. This technique leads to an inexact Newton's method, which uses the criterion defined in (2.23). In the case of η being 0, the criterion forces an exact algebraic solution of the Newton equation. As η increases, the iterative solver is permitted to reduce the number of iterations used and loosen the criterion for a solution. For more information about inexact Newton's method, see [2].

$$\|F(x) + F'(x)s\| \leq \eta \|F(x)\| \quad (2.23)$$

2.3.3 Globalization techniques

To address the second question, one must globalize the method. A globalization is a method that tests each step and, if necessary, modifies it to obtain an iterate that gives significant progress. To test progress, the method compares the actual and predicted norm reduction, as defined in (2.24) and (2.25).

$$Ared = \|F(x)\| - \|F(x + s)\| \quad (2.24)$$

$$Pred = \|F(x)\| - \|F(x) + F'(x)s\| \quad (2.25)$$

The test determines if s , the inexact Newton step, meets the criterion in (2.26). If it does, the algorithm accepts the step as valid and then takes another Newton step. If the step is invalid, the step size is decreased until the criterion is met.

$$Ared \geq t * Pred \quad (2.26)$$

In (2.26), t is a free parameter that can vary between zero and one; a typical value of t is 10^{-4} .

Globalization applied to an inexact Newton's method

When using an inexact Newton's method, an appropriate globalization criterion is (2.27).

$$\|F(x + s)\| \leq [1 - t(1 - \eta)] \|F(x)\| \quad (2.27)$$

Below is the full algorithm for the globalization used in the method, called the “Inexact Newton Backtracking” Method. Here, η is the parameter used to determine the accuracy of the solution of $F'(x)s = -F(x)$, θ is the parameter used to adjust the size of s to ensure progress towards the solution, and t is the parameter used to determine the tolerance of the step criterion.

- Given initial x , $t \in (0, 1)$, $\eta_{max} \in [0, 1)$, θ_{min} , and θ_{max} , $0 < \theta_{min} < \theta_{max} < 1$,
- Do the following at each iteration:
- Choose the initial η for (2.23).
- Evaluate $F(x+s)$
- While $\|F(x + s)\| > [1 - t(1 - \eta)] \|F(x)\|$
 - Choose θ in $[\theta_{min}, \theta_{max}]$
 - Update $s = \theta s$
 - Update $\eta = 1 - \theta(1 - \eta)$
 - Re-evaluate $F(x+s)$

Here are some notes on the algorithm used above:

1. The initial η is determined adaptively as in “Choice 1” of [5], to maintain agreement between $\|F(x + s)\|$ and $\|F(x) + F'(x)s\|$

2. Every iteration within the inner while-loop is called a backtrack; each set of backtracks completes one Newton iteration.
3. t is a measure of how tight the overall criterion should be
4. η adjusts at every iteration to ensure that s will still meet the inexact Newton condition even though the globalization has adjusted s .
5. $\|F(x)\|$ is only calculated once in each iteration loop, but $\|F(x + s)\|$ needs to be calculated at each backtrack, or adjustment of s .
6. Typical values for the parameters used in the INB method are:
 - $\eta_{max} = .9$
 - $t = 10^{-4}$
 - $\theta_{min} = .1$
 - $\theta_{max} = .5$
7. θ is chosen at each backtrack to minimize a quadratic that interpolates g , defined as $g(\theta) = \|F(x + \theta s)\|^2$, subject to $\theta_{min} \leq \theta \leq \theta_{max}$.

Some papers on this topic include [2], [4], and [5]. [2] formulates the basic inexact Newton method and develops local convergence analysis. [4] formulates the inexact Newton backtracking method. [5] formulates the adaptive procedure for determining the initial η .

2.3.4 Solving the linear Newton equation

The third question above addresses the selection of an iterative linear solver. Our choice of method in this project was the Generalized Minimal Residual Method, also known as GMRES. GMRES is a Krylov Subspace Method. The advantage to a Krylov method is that there is no need to directly calculate $F'(x)$; only products of $F'(x)$ and vectors are needed.

A Krylov subspace method for solving $Ax = b$ follows the following algorithm:

- Given an initial approximation x_0 .
- Set $r_0 = b - Ax_0$.
- Choose some $z_k \in K_k \equiv \text{span}(r_0, Ar_0, \dots, A^{k-1}r_0)$.
- Calculate $x_k = x_0 + z_k$.

The distinguishing characteristic among the various Krylov methods is the method for calculation of z_k ; in the case of GMRES, the criterion for choosing z_k is:

$$z_k = \text{argmin} \|b - A(x_0 + z)\| \tag{2.28}$$

2.3.5 Preconditioning

Preconditioning is the process of modifying a matrix equation in order to improve its solvability. The main indicator of improvement is called the condition number. For a general matrix equation, as in (2.29), the condition number is defined in (2.30).

$$Ax = b \tag{2.29}$$

$$\kappa = \|A\| \|A^{-1}\| \tag{2.30}$$

One type of preconditioning is right preconditioning; this is demonstrated with a conditioning matrix M in (2.31). Although the exact solution x doesn't change, the solvability properties of the new system with $A_{new} = M^{-1}A$ and $b_{new} = M^{-1}b$ have the potential to greatly improve.

$$M^{-1}Ax = M^{-1}b \tag{2.31}$$

In general, if the preconditioning matrix is chosen wisely, there will be a decrease in the number of iterations required for an iterative solver, but each iteration will become more expensive. There are many situations in which this tradeoff is worth it; Rayleigh-Benard convection happens to be one of those systems, as will be discussed in Chapter 3.

Chapter 3

Methodology

3.1 Discretization overview

In this section, there will be a discussion of how each variable and its corresponding derivatives were discretized in the solution process.

The goal of the discretization was to setup an effective way to calculate both the numerical approximation of the Jacobian for the linear Newton's step as well as the non-linear residual at each step.

3.1.1 Discretization of the temperature

Temperature had to be set on a grid with m rows and n columns of internal nodes, and it was also necessary to maintain the temperatures on the insulated sides of the grid, since the value of T is an unknown at these locations. Along the top and bottom boundaries of the grid, there are no unknowns specified, so we didn't need to worry about those locations. Hence the size of the temperature grid was m rows by $n+2$ columns.

To find $\frac{\partial T}{\partial x}$ terms, a horizontal finite difference scheme was used, found in (3.1).

$$\frac{\partial T}{\partial x} \approx \frac{T_{i,j+1} - T_{i,j-1}}{2dx} \quad (3.1)$$

To approximate $\frac{\partial T}{\partial y}$, a vertical finite difference setup was sufficient, found in (3.2). Along the sides, $\frac{\partial T}{\partial y}$ can be considered to be zero, because at these locations, $\frac{\partial T}{\partial y}$ is always multiplying a quantity of value zero, as found in the system equations.

$$\frac{\partial T}{\partial y} \approx \frac{T_{i+1,j} - T_{i-1,j}}{2dy} \quad (3.2)$$

The last temperature term was the Laplacian of temperature, ΔT . This term combined the use of vertical and horizontal finite differences, as in (3.3).

$$\Delta T \approx \frac{T_{i+1,j} + T_{i-1,j} - 2T_{i,j}}{dy^2} + \frac{T_{i,j+1} + T_{i,j-1} - 2T_{i,j}}{dx^2} \quad (3.3)$$

The Laplacian temperature term along the sides was necessarily set equal to zero because of (2.18). All the other terms in this equation go to zero because of the boundary conditions on ψ , so this term must as well.

3.1.2 Discretization of ψ , the stream function

For $\frac{\partial \psi}{\partial x}$, the central finite difference equation was used, just as in $\frac{\partial T}{\partial x}$ (see (3.1)). Along the boundaries, ψ is known to be zero from the boundary conditions, so the values of ψ are known. This allowed for the consideration of only interior nodes for all terms involving ψ , since the boundary nodes were already known.

For $\frac{\partial \psi}{\partial y}$, just as with $\frac{\partial \psi}{\partial x}$, a central finite difference formula was used (see (3.2)).

The last ψ term is the Laplacian. For this term, the same finite difference formula used for the temperature Laplacian was employed (see (3.3)).

3.1.3 Discretization of ω , vorticity

ω was the trickiest variable to discretize because of its relatively complicated boundary conditions. On the interior points of the grid, the same finite-difference formulas used for temperature and ψ were applied. However, along the edges of the interior grid, the formulas required values of ω from the boundaries which were not necessarily zero.

For $\frac{\partial \omega}{\partial x}$, the boundary values of ψ were needed along the left and right edges of the interior nodes. At the left edge of the interior points, applying the basic finite difference equation, (3.4) is obtained.

$$\frac{\partial \omega}{\partial x} \approx \frac{\omega_{i,2} - \omega_{i,bdry}}{2dx} \quad (3.4)$$

Since the value to the left of the point is unknown, we had to use (2.19), which states that $\omega = -\Delta\psi$. The second derivative of ψ with respect to y is zero, since ψ is known to be zero all along the edge. However, we needed to calculate the values of ψ to the left and right of the boundary. The left of the boundary was an imaginary node; however, the node to the right was a known value of ψ . Using the symmetry condition on ψ at the boundary, we can say that these two values are equal. Hence, we arrive at (3.5). In this equation, the column to the right of the boundary corresponds to $j = 1$, the first column of interior nodes.

$$\omega_{i,bdry} = -\Delta\psi \approx \frac{\psi_{i+1,bdry} + \psi_{i-1,bdry} - 2\psi_{i,bdry}}{dy^2} + \frac{\psi_{i,1} + \psi_{i,1} - 2\psi_{i,bdry}}{dx^2} \quad (3.5)$$

Since the values of ψ are zero along the boundary, (3.5) reduces to (3.6).

$$\omega_{i,bdry} = -\Delta\psi \approx \frac{2\psi_{i,1}}{dx^2} \quad (3.6)$$

Inserting (3.6) into (3.4), we arrive at (3.7).

$$\frac{\partial \omega}{\partial x} \approx \frac{\omega_{i,2} - \frac{2\psi_{i,1}}{dx^2}}{2dx} \quad (3.7)$$

(3.7) can then be used to approximate the derivatives of ω . A similar argument can be used for both the y derivative and the Laplacian terms.

3.2 Preconditioning

The trade-off in preconditioning is to balance the additional linear solve steps caused by preconditioning with the possibility of better overall performance in the Krylov solver and in the residual reduction of Newton's method. To test this on the system, two runs were setup for various mesh sizes (16x16, 24x24, 32x32, 48x48), with $\gamma = 1$ and $R_a = 3000$.

Pre-conditioning is clearly worth it in our case. The preconditioner was an incomplete LU factorization with drop tolerance .05 of the block diagonal part of the Jacobian matrix. Performance of the algorithm for $n = m = 32$ was improved about twenty-five percent, shaving the number of inexact Newton iterations from about 20 to about 15 (to achieve a residual norm of under .01). To show the effects of pre-conditioning on the system, two comparisons will be made. The first comparison, shown in Figure 3.1, shows the non-linear residual norm after each INB step for the system with and without preconditioning. Figure 3.2 tracks the linear residual norm within each step as a function of GMRES iterations; the sudden jumps in the graph represent discrepancy between the non-linear residual norm and the linear residual norm calculated within the iterative solver. Both of these figures clearly indicate the benefits of preconditioning; in fact, without preconditioning, convergence could not be achieved on a system with mesh size of 48x48.

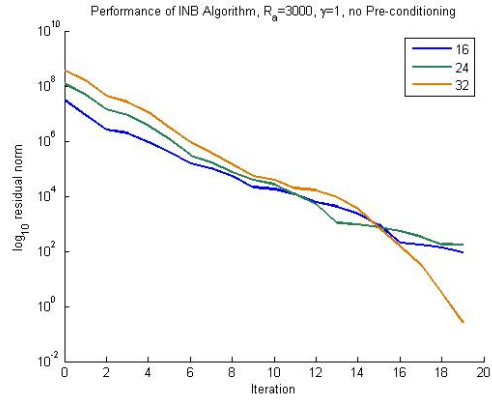
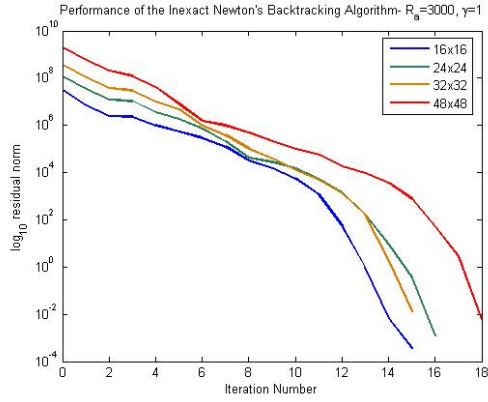


Figure 3.1: The effect of preconditioning on INB

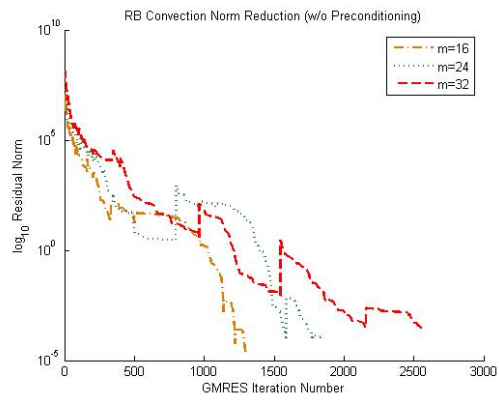
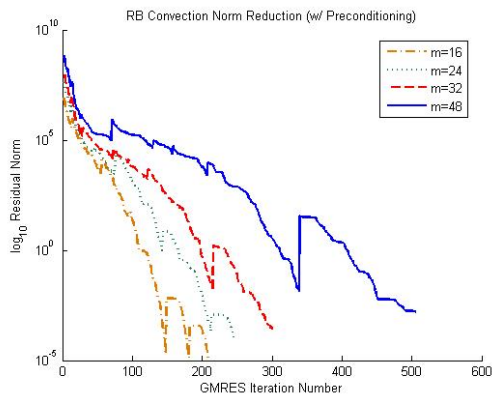


Figure 3.2: The effect of preconditioning on GMRES

Chapter 4

Results

4.1 Summary of linear stability results

[6] was the primary source for data regarding a linear stability analysis of the system equations. In this section, a brief overview of the results will be presented. Figure 4.1 is a graphical summary of the results obtained with respect to the two system variables Ra and γ . The author uses a different definition of Rayleigh number; the conversion is found as (4.1). The graph shows a prediction of what types of solutions will be present at various parameter values.

$$Ra = \left(\frac{2}{\gamma}\right)^4 R \quad (4.1)$$

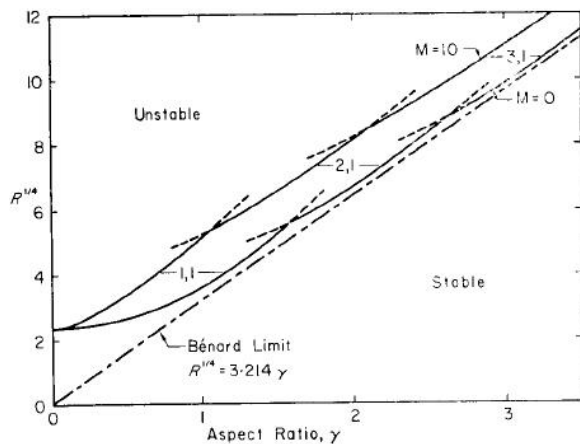


Figure 4.1: Curves of neutral stability under variables R and γ

The plots of several solutions obtained through the linear stability analysis are found in Figure 4.2. In the next section, these results will be compared with those found through the computation to ensure validity of the solutions.

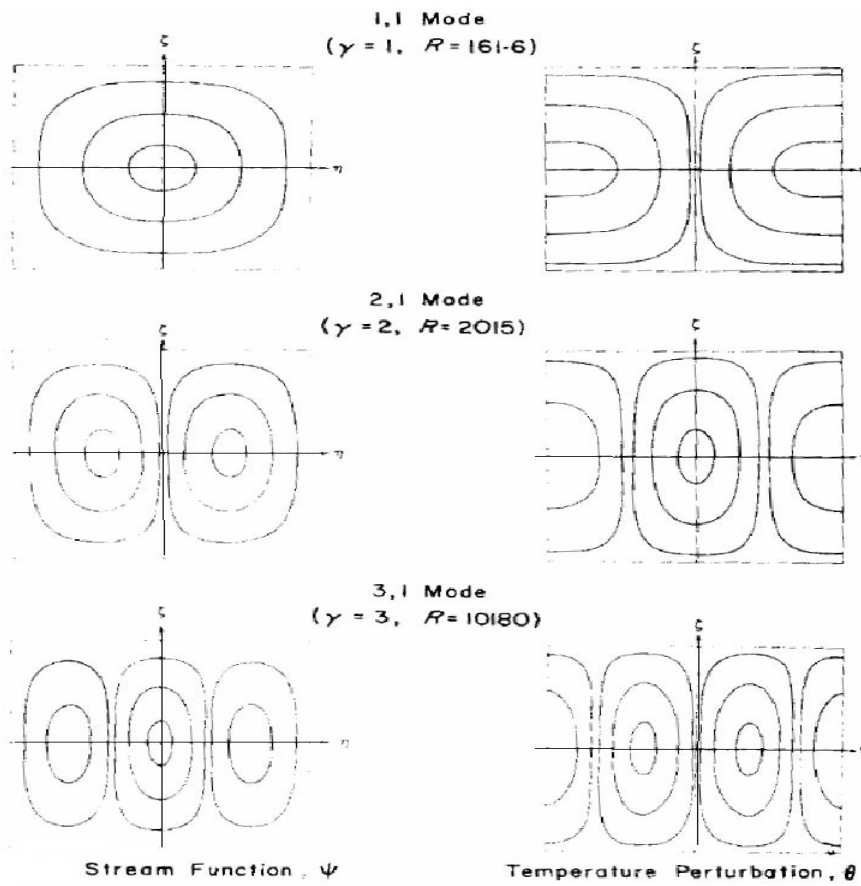


Figure 4.2: Sketches of solutions at various Ra and aspect ratio [6]

Mode	R from paper	Rayleigh Number
1	161.6	2585.6
2	2015	2015
3	10180	2011

Table 4.1: Rayleigh number conversion table

4.2 Solution

To verify that the solutions were valid, I compared the results from the computer simulation to the sketches provided in [6]. Figure 4.2 shows the sketches found in the reference. The results obtained through the computer simulations are shown in Figure 4.3. Table 4.1 has the values of both the paper R values and the Ra values used in the report.

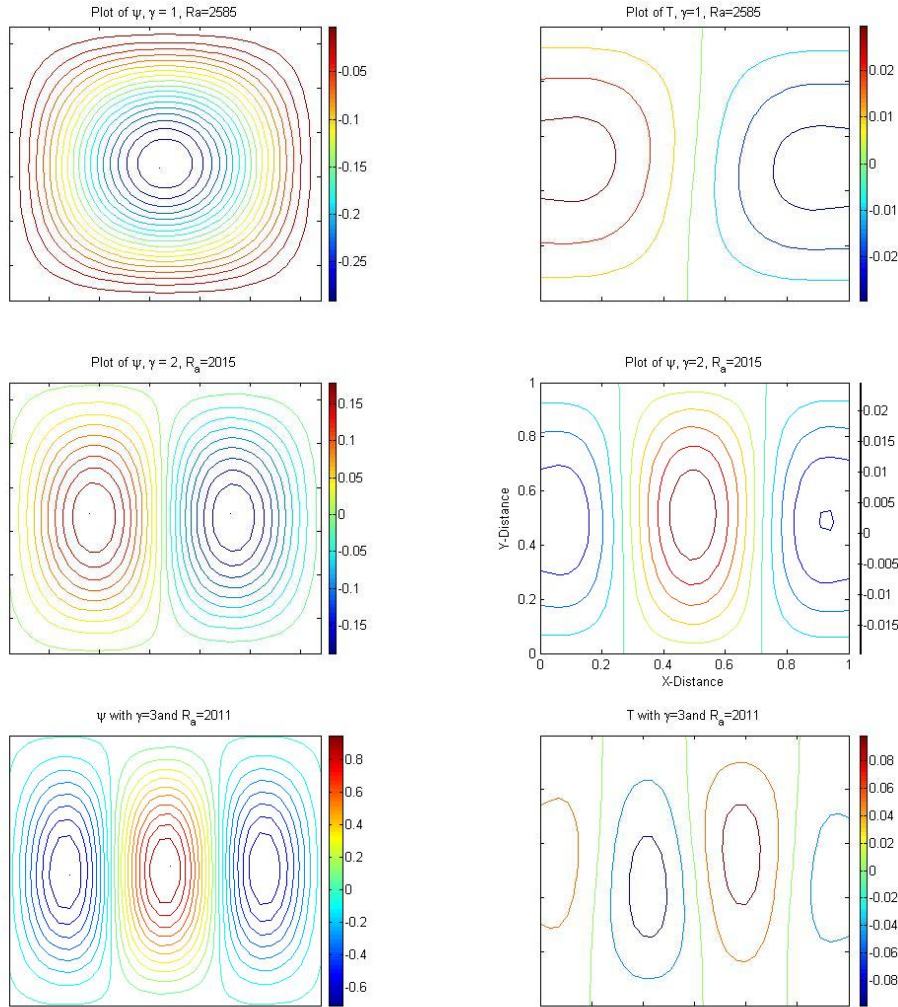


Figure 4.3: Solution obtained at various Ra and γ

As one can see from the figures, the results between the two match up very well, indicating that the computer simulation is working. However, there are some differences and discrepancies. First off, the temperature profiles from the computation do not approach the vertical walls completely perpendicular, as they should considering the boundary conditions. This is caused by numerical error, which is exag-

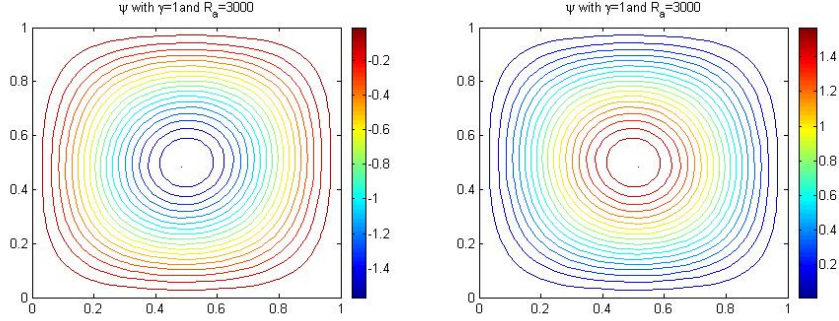


Figure 4.4: The two convection solutions

generated at larger aspect ratios, as seen in the steeper temperature gradient for aspect ratios of 2 and 3. The second difference to note is the oblong temperature profiles obtained in the computations vs the nice circles obtained through the linear stability analysis. Since the computations appear to satisfy the boundary conditions and the computational model made less approximations than the linear model, the true behavior is that obtained in the computational model. This can't be verified due to lack of experimental data, but it does illustrate that the linear model doesn't necessarily yield the correct physical results.

4.2.1 The presence of two convection solutions

In the problem where the parameters allow for convection, there are two solutions, corresponding to clockwise and counterclockwise flow. Each of these could be obtained in practice, depending on the initial conditions; both solutions satisfy all symmetries and boundary conditions. The ψ plot for both of these solutions can be found in Figure 4.4, for a Ra of 3000 and a γ of 1.

4.3 Symmetries in the solution

The first mode, which is a single circular roll, is fixed by $\kappa_1\kappa_2$, since the velocity and temperature profiles are symmetric across the main diagonal. Therefore, for mode 1, we should expect the following symmetries for ψ , ω , and T :

1. $\psi(L - x, 1 - y) = \psi(x, y)$
2. $\omega(L - x, 1 - y) = \omega(x, y)$
3. $T(L - x, 1 - y) = -T(x, y)$

For ψ , the symmetry is obtained, as seen in Figure 4.5. For T , the expected symmetry result also holds, as seen in Figure 4.6.

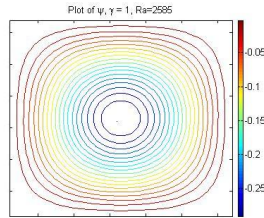


Figure 4.5: ψ of mode 1 as found with the computer simulation

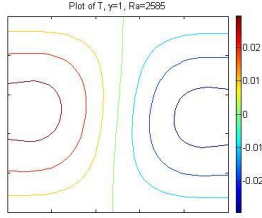


Figure 4.6: T of mode 1 as found with the computer simulation

For the second mode, there are two mirror image rolls next to each other along the x -direction. Therefore, symmetry with respect to a vertical midplane is expected (since the rolls would be mirror images on either side of this midplane), which corresponds to element κ_1 . Therefore, for mode 2, we should expect the following symmetries:

1. $\psi(L - x, 1 - y) = -\psi(x, y)$
2. $\omega(L - x, 1 - y) = -\omega(x, y)$
3. $T(L - x, 1 - y) = T(x, y)$

For ψ , one can see that the solution is symmetric across a midplane with opposite signs, as predicted, by examining Figure 4.7. For T , the temperature is symmetric across a midplane, as predicted. This can be seen in Figure 4.8 (for all of these figures, $\gamma = 2$).

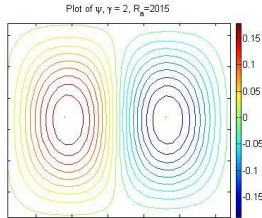


Figure 4.7: ψ of mode 2 as found with the computer simulation

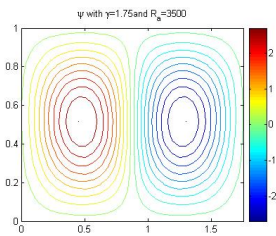


Figure 4.8: T of mode 2 as found with the computer simulation

4.4 Bifurcation results

4.4.1 Temperature amplitude as a function of Ra

This section will talk about the results in regard to continuation of the solution with respect to Ra number and tracking the amplitude. In order to examine the behavior of the system as the Rayleigh number is changed, a linear continuation was used. Here is the algorithm for this calculation:

1. Solve the solution at the first Ra
2. Record the maximum value of the temperature
3. Increase the value of Ra
4. Solve at the new Ra , using the results from the previous solve step as an initial guess

The curve obtained can be found in Figure 4.9.

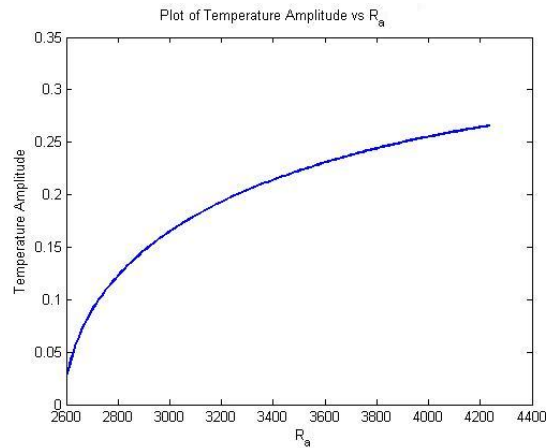


Figure 4.9: Amplitude of temperature perturbation as a function of Rayleigh number

4.4.2 Variation in aspect ratio, with a constant Ra

In addition to investigating what happens for a given aspect ratio γ as Ra increases, the solution was also obtained at various points in the Ra / γ plane. The initial data from the linear stability analysis were taken from [6], as discussed in section 4.1. A qualitative picture of the results is seen in Figure 4.10.

Let us choose a Ra number and increase γ , the aspect ratio. The diagram tells us that various modes will be found, until we reach the point at which Ra is not high enough to “sustain” that mode, and the zero solution will be found.

The journey begins with $Ra = 3500$ and $\gamma = 1$. Increasing γ while keeping Rayleigh constant, we expect a transition between the first mode (one roll) and the second mode (two rolls) at approximately $\gamma = 1.6$. As is shown in Figure 4.11, this transition occurs, as expected; the solution is also shown for several intermediate and following values of γ . At $\gamma = 1.6$, there is also a mixed-mode solution, or combination of both mode 1 and mode 2 solutions.

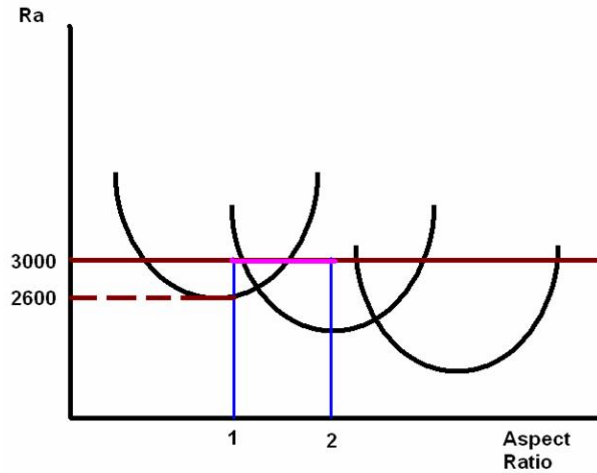


Figure 4.10: Qualitative graph of neutral stability curves under variables R and γ

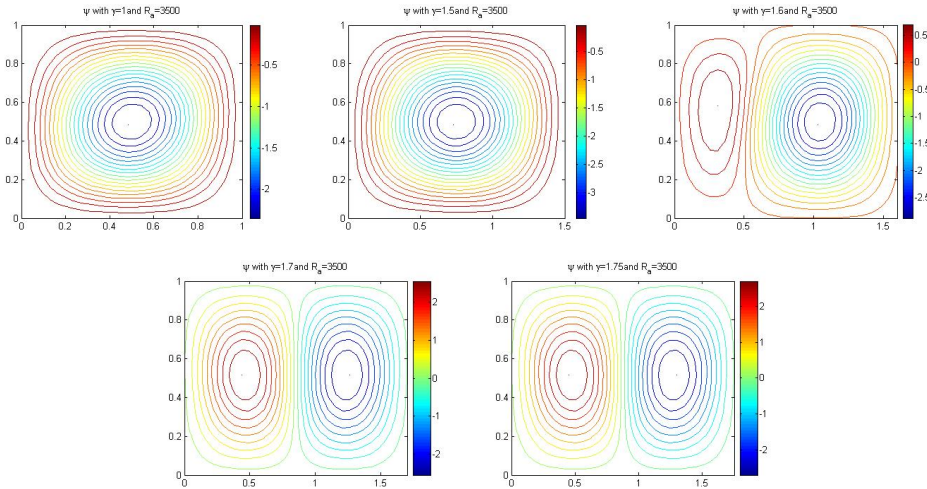


Figure 4.11: A “journey” across various γ for $Ra = 3500$

4.5 Animation program

A side project of the MQP was to create a fluid animation program that could accept a velocity field as an input and show the motion of particles along the contours. The goal of the side project was two-fold; first, it would provide an experience in how to program fluid motion. Secondly, it would aid as a visualization tool for the MQP presentation to be delivered at the end of the year.

The numerical method used was a Runge-Kutta method; this is an advanced differential equations solver that calculates the future position of a particle based on its current and past values. At first, a simple Euler’s method was attempted, which uses only the current position and velocity to calculate the next position, but this method proved insufficient, and caused all of the particles to drift to the outside of the domain (since for circular contours, the velocity will always move the particle to a larger radius).

Even with the more advanced method, there were still errors, but the fluid animation program could not be advanced further due to time constraints. A screen shot of the animation program can be found in Figure 4.12.

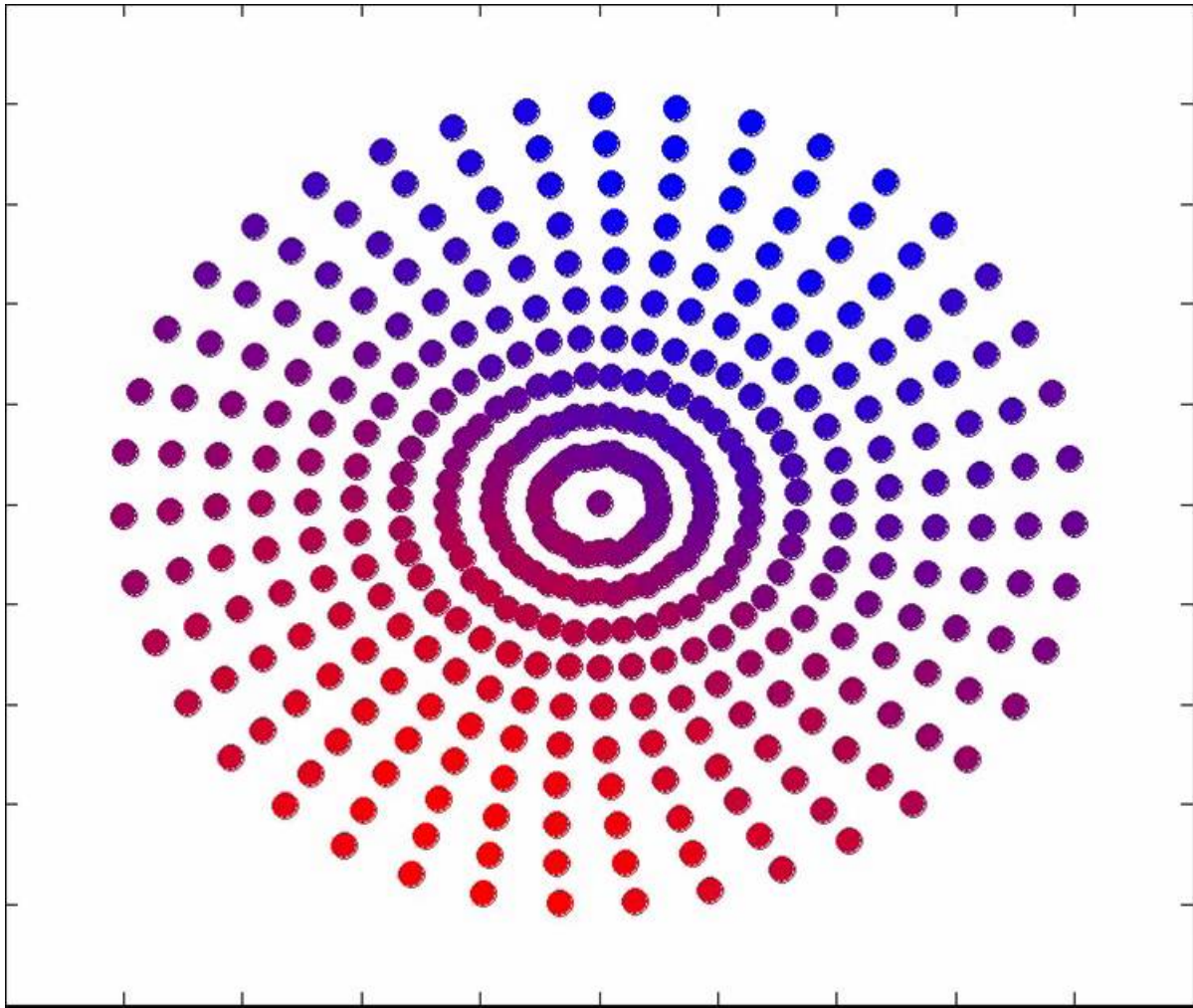


Figure 4.12: Screenshot of the animation program

Chapter 5

Conclusions and Future Work

5.1 Conclusions

1. The programs written were valid, agreeing with experimental and analytical work.
2. The linear analytical model doesn't necessarily capture the behavior of the system, as seen in the slight disagreements between the plots obtained from linear stability analysis and computations
3. The computational model predicted a bifurcation of the convection solution (Mode 1) around $Ra = 2600$, as found in experiments and the analytical model.

5.2 Future Work

1. Continue solutions computationally in two parameters, aspect ratio and Rayleigh number; in our trials, continuation was only done with respect to one variable.
2. Complete an analysis of solutions with respect to time, extending the problem beyond only steady-state solutions.

Bibliography

- [1] S. Chandrasekhar. *Hydrodynamic and Hydromagnetic Stability*. Dover, New York, 1981.
- [2] R. S. Dembo, S. C. Eisenstat, and T. Steihaug. Inexact Newton methods. *SIAM J. Numer. Anal.*, 19:400–408, 1982.
- [3] J. E. Dennis, Jr. and R. B. Schnabel. *Numerical Methods for Unconstrained Optimization and Nonlinear Equations*. Series in Automatic Computation. Prentice-Hall, Englewood Cliffs, NJ, 1983.
- [4] S. C. Eisenstat and H. F. Walker. Globally convergent inexact Newton methods. *SIAM J. Optimization*, 4:393–422, 1994.
- [5] S. C. Eisenstat and H. F. Walker. Choosing the forcing terms in an inexact Newton method. *SIAM J. Sci. Comput.*, 17:16–32, 1996.
- [6] U.H. Kurzweg. Convective instability of a hydromagnetic fluid within a rectangular cavity. *International Journal of Heat Mass Transfer*, 8:35, 1965.